

Limits on mass outflow from optical tidal disruption events

Tatsuya Matsumoto^{1,2,3}*† and Tsvi Piran¹

¹*Racah Institute of Physics, Hebrew University, Jerusalem, 91904, Israel*

²*Research Center for the Early Universe, Graduate School of Science, University of Tokyo, Tokyo 113-0033, Japan*

³*Department of Physics, Graduate School of Science, University of Tokyo, Tokyo 113-0033, Japan*

26 January 2021

ABSTRACT

The discovery of optical/UV tidal disruption events (TDEs) was surprising. The expectation was that, upon returning to the pericenter, the stellar-debris stream will form a compact disk that will emit soft X-rays. Indeed the first TDEs were discovered in this energy band. A common explanation for the optical/UV events is that surrounding optically-thick matter reprocesses the disk’s X-ray emission and emits it from a large photosphere. If accretion follows the super-Eddington mass infall rate it would inevitably result in an energetic outflow, providing naturally the reprocessing matter. We describe here a new method to estimate, using the observed luminosity and temperature, the mass and energy of outflows from optical transients. When applying this method to a sample of supernovae our estimates are consistent with a more detailed hydrodynamic modeling. For the current sample of a few dozen optical TDEs the observed luminosity and temperature imply outflows that are significantly more massive than typical stellar masses, posing a problem to this common reprocessing picture.

Key words: radiation mechanisms: thermal, (stars:) supernovae:general, transients: supernovae, transients: tidal disruption events

1 INTRODUCTION

A tidal disruption event (TDE) occurs when a star approaches a supermassive black hole (BH) in a galactic center and reaches the tidal radius where the tidal force is strong enough to overcome the star’s self-gravity. After the disruption, about half of the stellar debris is unbound. The other bound half falls back to the BH with a fallback rate $\dot{M}_{\text{fb}} \propto t^{-5/3}$ (Rees 1988; Phinney 1989). Upon returning to the pericenter, if the fallback stream circularized rapidly it will form a compact accretion disk. A disk of this size will produce soft X-ray/UV emissions. About ten TDEs, whose location is consistent with the center of their host galaxies and their light curve decays as the accretion rate $\propto t^{-5/3}$, have been detected in the soft X-ray band by the ROSAT survey (Brandt et al. 1995; Grupe et al. 1995; Bade et al. 1996; Grupe et al. 1999; Komossa & Bade 1999; Komossa & Greiner 1999; Greiner et al. 2000), XMM-Newton (Esquej et al. 2007, 2008), and Chandra (Maksym et al. 2013; Donato et al. 2014, see Komossa 2015 for a review of these early observations).

A different class of TDEs, hereafter denoted “optical TDEs”, was discovered in the last decade in optical and UV bands. Like the earlier X-ray TDEs these events are also located in galactic nuclear regions and their light curves decline roughly as $t^{-5/3}$. A few dozen such events have been detected by wild-field high-cadence optical/UV surveys, such as GALEX (Gezari et al. 2006, 2008), SDSS (van Velzen et al. 2011), pan-STARRS (Gezari et al. 2012; Chornock et al. 2014), PTF (Arcavi et al. 2014), iPTF (Blagorodnova et al. 2017, 2019; Hung et al. 2017), and ASASSN (Holoien et al. 2014,

2016a,b). Recently, ZTF almost doubled the sample size (van Velzen et al. 2020a; Nicholl et al. 2020).

Common characteristics of optical TDEs that are most relevant to this work are (Hung et al. 2017; van Velzen et al. 2020a,b): (i) a peak bolometric luminosity $L \sim 10^{44}$ erg s⁻¹, (ii) a typical duration longer than $t \gtrsim 100$ days, (iii) a black-body temperature of $T \approx 3 \times 10^4$ K that does not vary much during the observation. (iv) spectra dominated by a blue continuum component. Some events show broad emission lines corresponding to the velocity of $v \lesssim 10^4$ km s⁻¹ (Arcavi et al. 2014). (v) a total emitted energy $Lt \sim 10^{51}$ erg that is much lower than the expected total energy from efficient accretion of a solar mass onto a BH ($\sim 10^{53}$ erg) or even from the energy required to circularize the flow onto an accretion disk ($\sim 10^{52}$ erg). This is the so-called “inverse energy crisis” (Piran et al. 2015; Stone & Metzger 2016; Lu & Kumar 2018).

These properties of optical TDEs are inconsistent with the classical picture in which soft X-rays from an accretion disk are expected to dominate the emission. Instead, it was proposed that the emission is reprocessed by surrounding matter. Strubbe & Quataert (2009); Lodato & Rossi (2011) proposed an outflow launched from small radii (probably a super-Eddington disk wind) radiating away its thermal energy. Later on others (Metzger & Stone 2016; Roth et al. 2016; Roth & Kasen 2018; Dai et al. 2018; Lu & Bonnerot 2020; Piro & Lu 2020) proposed that an outflow (either a super-Eddington disk wind or the result of shocks in stream-stream or stream-disk collisions) expands, remains optically thick, and reprocesses the ionizing continuum from the inner accretion disk. We denote these as “reprocessing-outflow” models. Since the fallback rate is much larger than the Eddington rate, super-Eddington emission (Loeb & Ulmer 1997; Krolik & Piran 2012) and an outflow from the disk (e.g.,

* E-mail: tatsuya.matsumoto@mail.huji.ac.il

† JSPS Research Fellow

(Blandford & Begelman 1999) are naturally expected. The expanding material surrounds the system and reprocesses the soft X-rays emitting photons in optical/UV band if thermalization is efficient (Roth et al. 2016; Roth & Kasen 2018). Metzger & Stone (2016) have suggested that the outflow carries out a significant fraction of the infalling mass, reducing the mass accreted by the BH and hence the energy generation rate. Alternatively, the outflow can carry out the excess energy in the form of kinetic energy. This would have resolved the “inverse energy crisis” (Piran et al. 2015; Stone & Metzger 2016; Lu & Kumar 2018).

An alternative model (Piran et al. 2015; Krolik et al. 2016) suggests that the observed optical emission is generated by interactions between the bound stellar debris taking place around the apocenter. This model follows the simulations of Shiokawa et al. (2015) who have shown that the fallback stream passes the pericenter without forming a disk and it collides with the debris near the apocenter. Heated by shocks, the interacting part powers the observed optical emission (see also Svirski et al. 2017; Ryu et al. 2020). In this case the accretion onto the BH is delayed and is possibly inefficient.

In this work we focus on the former scenario in which we expect an outflow that is relevant to the reprocessing process. Following recent works by Shen et al. (2015) and Piro & Lu (2020), we analyze the condition within the emitting region and estimate the ejecta mass involved in the optical TDEs. We then impose the condition that this mass cannot exceed the disrupted stellar mass, which is of order of a solar mass and explore its implications on the reprocessing model. We organize the paper as follows. In §2, we develop the method to estimate the ejecta mass of optical transients in a general quasi-spherical optically thick situation using the observed luminosity and temperature. In §3, we apply this method to supernovae (SNe) and confirm that we can estimate the ejecta mass with a good accuracy. In §4, we calculate the ejecta mass of available optical TDEs by assuming that the emission is powered by spherically expanding wind. We summarize our result and their implications in §5.

2 METHOD

We construct a framework to estimate ejecta mass of optical transients assuming that (i) they expand quasi-spherically and (ii) they are optically thick. The observed photons are thermal and diffuse out of the ejecta. In the context of optical TDEs this situation arises within the “reprocessing-outflow” model. We note that our framework is relevant not only to explosive phenomena like SNe and other transients (Piro & Lu 2020; Uno & Maeda 2020), but also to quasi-steady-state configurations as was discussed in Shen et al. (2015) for the ultraluminous X-ray source M101 X-1.

We begin defining two critical radii that determine the observables (e.g., Nakar & Sari 2010; Shen et al. 2015). The first is the diffusion radius, R_d , (denoted photon trapping radius, R_{trap} , by Shen et al. 2015) above which the photon diffusion time is shorter than the dynamical time and photons can freely escape from the ejecta. Using the total optical depth we write this condition as

$$\tau(R_d) \equiv \int_{R_d}^{\infty} (\kappa_{\text{es}} + \kappa_a) \rho dR = \frac{c}{v_d}, \quad (1)$$

where κ_{es} and κ_a are the Thomson (electron scattering) and absorption opacities, ρ is the density, c is the speed of light, and v_d is the ejecta velocity at R_d .

The color radius, R_c , (denoted thermalization radius, R_{th} , by Shen et al. 2015) is the location where the photons’ last absorption occurs (namely, photons are in thermal equilibrium with the gas within R_c).

This radius is defined by the effective optical depth as (Rybicki & Lightman 1979):

$$\tau_{\text{eff}}(R_c) \equiv \int_{R_c}^{\infty} \sqrt{\kappa_a(\kappa_{\text{es}} + \kappa_a)} \rho dR = 1. \quad (2)$$

Strictly speaking, photons with different energies will have different effective optical depths. We define the color radius as the radius corresponding to the observed color temperature (see Shen et al. 2015; Lu & Bonnerot 2020, for details). In order to derive this radius, we use for κ_a the Planck-mean absorption opacity.

The system has two different physical situations depending on whether $R_d > R_c$ or $R_c > R_d$. In the former case, photons are trapped within the ejecta and advected up to R_d . The observed luminosity is given by the diffusion luminosity there. The observed color temperature is given by the photon temperature at R_d , which is the same as the gas temperature.¹ When $R_c > R_d$, photons diffuse out from R_d but they are still thermally coupled to the gas. The observed color temperature is determined by the radiation temperature at R_c . Fig. 1 depicts a schematic picture of the system we consider for the cases of $R_d > R_c$ and $R_d < R_c$.

Using the observed luminosity L , temperature T , and the outflow velocity (when it is available) we can estimate the conditions at $R = \max(R_d, R_c)$ and using them we calculate the mass outflow rate passing through this radius:

$$\dot{M} = 4\pi R^2 \rho \left(v - \frac{dR}{dt} \right), \quad (3)$$

where v is the ejecta velocity at R . The last term dR/dt arises because the radii R_d and R_c move in both the Eulerian and Lagrangian (mass) coordinates. Usually, as the ejecta expand, these radii recede in the mass coordinate. Integrating the mass outflow rate over time we calculate the total ejecta mass above this radius.

To determine R_d and R_c we use the simplified forms of Eqs. (1) and (2). For the absorption opacity, we adopt the Kramers’ opacity $\kappa_a = \kappa_0 \rho T_g^{-7/2}$ for TDEs, where κ_0 is a constant that depends on the composition and T_g is the gas temperature. Since the absorption opacity is always smaller than the Thomson opacity ($\kappa_a \ll \kappa_{\text{es}}$), and as long as the density profile is steeper than $\rho \propto r^{-1}$, we can approximate the optical depths in Eqs. (1) and (2) and obtain:

$$\tau(R_d) \approx \kappa_{\text{es}} \rho_d R_d = c/v_d, \quad (4)$$

$$\tau_{\text{eff}}(R_c) \approx \sqrt{\kappa_{\text{es}} \kappa_a} \rho_c R_c = 1, \quad (5)$$

where ρ_d and ρ_c are the density at R_d and R_c , respectively. For TDEs in which the chemical abundance is solar and temperatures are $\approx 3 \times 10^4$ K we use $\kappa_{\text{es}} = 0.35 \text{ cm}^2 \text{ g}^{-1}$ and $\kappa_0 = 4 \times 10^{25}$. We also use these values as fiducial values in the rest of this section. When we analyze type Ic SNe in §3, whose temperatures are much lower and whose ejecta are hydrogen and helium free, we use $\kappa_{\text{es}} = 0.07 \text{ cm}^2 \text{ g}^{-1}$ and a constant absorption opacity of $\kappa_a = 0.01 \text{ cm}^2 \text{ g}^{-1}$ (see Appendix A for details of our opacity prescription).

The mass outflow rate (Eq. 3) depends on whether $R_d > R_c$ or $R_c > R_d$. In the former case, the observed luminosity and color temperature are determined at R_d . The bolometric luminosity is given by the diffusion approximation at R_d :

$$L = -\frac{4\pi R_d^2 a c}{3\kappa_{\text{es}} \rho_d} \frac{dT^4}{dR} \approx \frac{4\pi R_d^2 a v_d T^4}{3}, \quad (6)$$

¹ Note that beyond R_c the photons and the gas cool adiabatically as $T \propto \rho^{1/3}$ and $T_g \propto \rho^{2/3}$, respectively. However, Compton heating will heat the gas to the same temperature as the radiation in radiation-pressure-dominated ejecta.

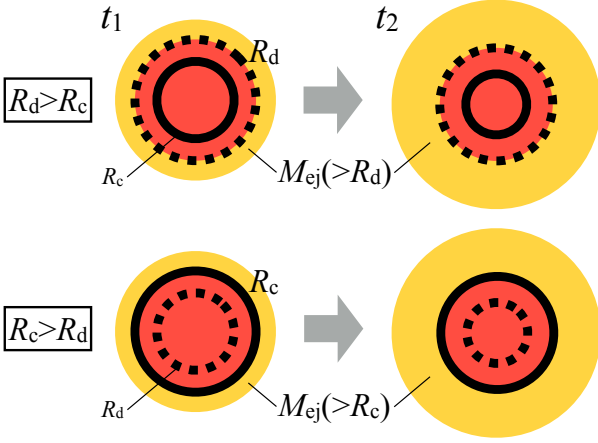


Figure 1. A schematic picture of system at two time $t_1 < t_2$ for the two different cases. (**Top**) $R_d > R_c$, photons are trapped within the ejecta up to the diffusion radius (R_d , dotted curve) and escape from the regions beyond R_d (marked by yellow color). (**Bottom**) $R_c > R_d$, photons diffuse out of the ejecta beyond R_d , but they are still in thermal equilibrium with the gas up to the color radius (R_c , solid curve). Outside of R_c (also marked by yellow color), the photons decouple from the gas. As time progresses, both radii R_d and R_c shrink in the Lagrangian (mass) coordinate. Integrating over time the mass outflow rate \dot{M} at R_d and R_c , we estimate the ejecta mass that crossed R_d , $M_{\text{ej}}(>R_d)$ for the first case and the mass that crossed R_c , $M_{\text{ej}}(>R_c)$ for the second.

where a is the radiation constant and we used Eq. (4). Solving this equation for R_d , we obtain

$$R_d \simeq \left(\frac{3c}{2^4 \pi \sigma_{\text{SB}}} \right)^{1/2} L^{1/2} T^{-2} v_d^{-1/2}, \quad (7)$$

where $\sigma_{\text{SB}} = ac/4$ is the Stefan-Boltzmann constant. Combining this equation with Eq. (4), we estimate ρ_d :

$$\rho_d \simeq \left(\frac{2^4 \pi c \sigma_{\text{SB}}}{3 \kappa_{\text{es}}^2} \right)^{1/2} L^{-1/2} T^2 v_d^{-1/2}. \quad (8)$$

Combined together, the mass outflow rate at R_d is given by

$$\begin{aligned} \dot{M}_d &\simeq \left(\frac{3\pi c^3}{\kappa_{\text{es}}^2 \sigma_{\text{SB}}} \right)^{1/2} L^{1/2} T^{-2} v_d^{-1/2} f_d \\ &\simeq 8.3 \times 10^{-1} M_{\odot} \text{ day}^{-1} L_{44}^{1/2} T_4^{-2} v_{d,9}^{-1/2} f_d, \end{aligned} \quad (9)$$

$$f_d = 1 - \frac{dR_d}{v_d} = 1 - \frac{R_d}{v_d} \left(\frac{1}{2} \frac{d \ln L}{dt} - 2 \frac{d \ln T}{dt} - \frac{1}{2} \frac{d \ln v_d}{dt} \right), \quad (10)$$

where we use the convention of $Q_x = Q/10^x$ (in cgs units).

We turn to the case of $R_c > R_d$, in which photons are coupled to the gas up to R_c and the observed photon temperature equals to the gas temperatures at R_c , $T = T_g$. We can still use the diffusion approximation at R_c ² and the bolometric luminosity is given by

$$L = -\frac{4\pi R_c^2 ac}{3\kappa_{\text{es}} \rho_c} \frac{dT^4}{dR} \sim \frac{4\pi R_c ac T^4}{3\kappa_{\text{es}} \rho_c}. \quad (11)$$

² When $\tau_{\text{eff}}(R_c) = 1$, we have $\tau(R_c) = (\kappa_{\text{es}}/\kappa_a)^{1/2} > 1$.

Combining this equation with Eq. (5), we estimate R_c and ρ_c :

$$\rho_c = \left(\frac{2^8 \pi^2 \sigma_{\text{SB}}^2}{3^2 \kappa_{\text{es}}^3 \kappa_0} \right)^{1/5} L^{-2/5} T^{23/10}, \quad (12)$$

$$R_c = \left(\frac{3^3 \kappa_{\text{es}}^2}{2^{12} \pi^3 \kappa_0 \sigma_{\text{SB}}^3} \right)^{1/5} L^{3/5} T^{-17/10}. \quad (13)$$

Finally, the mass outflow rate at R_c is given by

$$\begin{aligned} \dot{M}_c &\simeq \left(\frac{3^4 \pi \kappa_{\text{es}}}{2^6 \kappa_0^3 \sigma_{\text{SB}}^4} \right)^{1/5} L^{4/5} T^{-11/10} v_c f_c \\ &\simeq 3.2 \times 10^{-1} M_{\odot} \text{ day}^{-1} L_{44}^{4/5} T_4^{-11/10} v_{c,9} f_c, \end{aligned} \quad (14)$$

$$f_c = 1 - \frac{dR_c}{v_c} = 1 - \frac{R_c}{v_c} \left(\frac{3}{5} \frac{d \ln L}{dt} - \frac{17}{10} \frac{d \ln T}{dt} \right), \quad (15)$$

where v_c is the ejecta velocity at R_c .

When $R_d > R_c$, the effective optical depth at R_d is smaller than unity $\tau_{\text{eff}}(R_d) < 1 (= \tau_{\text{eff}}(R_c))$ because the optical depth is a decreasing function of radius. With Eqs. (7) and (8) and taking into account the fact that the gas and photon temperatures are the same at R_d , we estimate the effective optical depth by

$$\tau_{\text{eff}}(R_d) \simeq \left(\frac{2^4 \pi \kappa_0^2 c^5 \sigma_{\text{SB}}}{3 \kappa_{\text{es}}^4} \right)^{1/4} L^{-1/4} T^{-3/4} v_d^{-5/4}. \quad (16)$$

Therefore, the condition $\tau_{\text{eff}}(R_d) < 1$ is rewritten as a condition on the velocity (see also Shen et al. 2015):

$$\begin{aligned} v_d > v_{\text{crit}} &\equiv \left(\frac{2^4 \pi \kappa_0^2 c^5 \sigma_{\text{SB}}}{3 \kappa_{\text{es}}^4} \right)^{1/5} L^{-1/5} T^{-3/5} \\ &\simeq 1.9 \times 10^4 \text{ km s}^{-1} L_{44}^{-1/5} T_4^{-3/5}, \end{aligned} \quad (17)$$

where we used $\rho_d < \rho_c$. Similarly, we find the condition for $R_c > R_d$ to be $v_c < v_{\text{crit}}$. It should be noted that we might not be able to determine v_d and v_c from observations (e.g., using line broadening because different lines are formed at different radii expanding at different velocities). Thus we determine which radius is larger by using an observed velocity v representative of the outflow velocity. Unless the velocity profile changes drastically within the ejecta, we determine the situation according to whether $v \geq v_{\text{crit}}$.

The ejecta mass above the radius $R = \max(R_d, R_c)$ is obtained by integrating Eq. (9) or (14) over time:

$$M_{\text{ej}}(>R) \simeq \int dt \dot{M}(L, T, v). \quad (18)$$

Similarly, the kinetic energy of ejecta is given by

$$E_{\text{kin}}(>R) \simeq \int dt \dot{M}(L, T, v) v^2 / 2. \quad (19)$$

The upper limit of the integrals should be the time when the radius reaches the center of the ejecta (the beginning of nebular phase). Although this time is difficult to identify in observations, the results do not depend sensitively on the choice of the time because the mass outflow rate declines after the peak of luminosity (see Figs. 2 and 5).

The maximal mass outflow rate is realized when $R_d = R_c$ and $v_d = v_c = v_{\text{crit}}$ (see also Shen et al. 2015)³:

$$\begin{aligned} \dot{M}_{\text{max}} &= \left(\frac{3^3 \pi^2 c^5}{2^2 \kappa_0 \kappa_{\text{es}}^3 \sigma_{\text{SB}}^3} \right)^{1/5} L^{3/5} T^{-17/10} f_d \\ &\simeq 6.0 \times 10^{-1} M_{\odot} \text{ day}^{-1} L_{44}^{3/5} T_4^{-17/10} f_d. \end{aligned} \quad (20)$$

³ Note that at v_{crit} , $f_d = f_c$.

3 APPLICATION TO SUPERNOVAE

We apply the method developed in the previous section to a sample of SNe with good data that have been analyzed using detailed numerical simulation (Taddia et al. 2018). We compare our results and verify that our method gives a reasonable estimate of the ejecta mass.

We consider a sample of type Ic SNe. For type II SNe, it is well known that the electron scattering opacity decreases drastically due to the hydrogen recombination at the color radius (e.g., Grassberg et al. 1971; Popov 1993; Faran et al. 2019). For type IIb and Ib SNe, most helium recombines shortly after the explosion ($\lesssim 10$ days, Dessart et al. 2011; Piro & Morozova 2014) due to its high recombination temperature. Such an early observation is not always performed and we miss most of the helium ejecta. used Thus, in this work, we focus on type Ic SNe for which the ejecta recombination is unimportant and we can ignore the temporal evolution of the electron scattering opacity adopting $\kappa_{\text{es}} = 0.07 \text{ cm}^2 \text{ g}^{-1}$ (see e.g., Lyman et al. 2016; Taddia et al. 2018, who estimated the ejecta masses of type Ic SNe using Arnett’s rule). The absorption opacity is dominated by bound-bound transitions because the ejecta are mainly composed of metals (Dessart et al. 2015). Here we use a constant absorption opacity $\kappa_{\text{a}} = 0.01 \text{ cm}^2 \text{ g}^{-1}$ (see appendix A). Note that when discussing SNe, here, we use a different absorption opacity prescription and opacity values than those used in §2.

When the ejecta expand homologously after the explosion (as in the case of SNe) we can simplify further the formula for the outflows. In this case, we can estimate the ejecta velocity at R by $v = R/t$, where t is the time measured since the explosion. We can then rewrite the mass formula using the observed time instead.

For the case of $R_{\text{d}} > R_{\text{c}}$, the velocity and outflow rate are given by

$$v_{\text{d}} = \left(\frac{3c}{2^4 \pi \sigma_{\text{SB}}} \right)^{1/3} L^{1/3} T^{-4/3} t^{-2/3} \quad (21)$$

$$\approx 7.5 \times 10^4 \text{ km s}^{-1} L_{42}^{1/3} T_4^{-4/3} t_{\text{day}}^{-2/3},$$

$$\dot{M}_{\text{d}} = \left(\frac{2^2 3 \pi^2 c^4}{(\kappa_{\text{es}} + \kappa_{\text{a}})^3 \sigma_{\text{SB}}} \right)^{1/3} L^{1/3} T^{-4/3} t^{1/3} f_{\text{d}} \quad (22)$$

$$\approx 1.3 \times 10^{-1} \text{ M}_{\odot} \text{ day}^{-1} L_{42}^{1/3} T_4^{-4/3} t_{\text{day}}^{1/3} f_{\text{d}},$$

$$f_{\text{d}} = \frac{2}{3} \left(1 - \frac{1}{2} \frac{d \ln L}{d \ln t} + 2 \frac{d \ln T}{d \ln t} \right), \quad (23)$$

where $t_{\text{day}} = t / \text{day}$. For $R_{\text{c}} > R_{\text{d}}$, the velocity and mass outflow rate are given by

$$v_{\text{c}} = \left(\frac{3^2 (\kappa_{\text{es}} + \kappa_{\text{a}})}{2^8 \pi^2 \sigma_{\text{SB}}^2 \kappa_{\text{a}}} \right)^{1/4} L^{1/2} T^{-2} t^{-1} \quad (24)$$

$$\approx 6.3 \times 10^4 \text{ km s}^{-1} L_{42}^{1/2} T_4^{-2} t_{\text{day}}^{-1}$$

$$\dot{M}_{\text{c}} = \frac{3}{2^2 \kappa_{\text{a}} \sigma_{\text{SB}}} L T^{-4} t^{-1} f_{\text{c}} \quad (25)$$

$$\approx 6.6 \times 10^{-2} \text{ M}_{\odot} \text{ day}^{-1} L_{42} T_4^{-4} t_{\text{day}}^{-1} f_{\text{c}},$$

$$f_{\text{c}} = \left(1 - \frac{1}{2} \frac{d \ln L}{d \ln t} + 2 \frac{d \ln T}{d \ln t} \right). \quad (26)$$

Instead of the critical velocity in Eq. (17), we introduce a critical time before (after) which $R_{\text{d}} > R_{\text{c}}$ ($R_{\text{c}} > R_{\text{d}}$) by equating v_{d} with

v_{crit} as

$$t_{\text{crit}} = \left(\frac{3^2 (\kappa_{\text{es}} + \kappa_{\text{a}})^3}{2^8 \pi^2 \kappa_{\text{a}}^3 \sigma_{\text{SB}}^2 c^4} \right)^{1/4} L^{1/2} T^{-2} \quad (27)$$

$$\approx 6.0 \times 10^{-1} \text{ day } L_{42}^{1/2} T_4^{-2},$$

To estimate the velocity accurately, we have to know the moment of the explosion. This is not always well-constrained by the observations, resulting in one of our largest sources of error.

First we analyze a well-observed SN 2004fe analyzed by Taddia et al. (2018). Fig. 2 depicts the time evolution of the bolometric luminosity, color temperature, calculated color radius, mass outflow rate at R_{c} , and ejecta mass out of R_{c} . For this and the following other SNe, R_{c} is always larger than R_{d} ($t_{\text{crit}} \lesssim \text{day}$). The mass outflow rate peaks around ≈ 25 days that reflects the time evolution of R_{c} . To see this effect, we also show \dot{M} and M_{ej} neglecting the term dR/dt ($f_{\text{c}} = 1$) with dashed curves (bottom two panels). When R_{c} expands (shrinks) with time, \dot{M} is suppressed (enhanced) from its value with $f_{\text{c}} = 1$ (that ignores this effect). This changes M_{ej} by up to $\sim 10\%$ (bottom panel). In Table 1, we show the resulting ejecta mass and kinetic energy. For a comparison, we also show the ratios of our results (M_{ej} , E_{kin}) to the values ($M_{\text{ej,Hy}}$, $E_{\text{kin,Hy}}$) obtained by one-dimensional hydrodynamic simulations with flux-limited diffusion (Taddia et al. 2018, see also Bersten et al. 2011, 2012 for the details of the calculation). Our results agree with those of the hydrodynamic modeling within a factor of 2. The errors are calculated by considering the uncertainty of the explosion time (other uncertainties such as the luminosity and temperature are not available in the literature and are neglected here).

We calculate the ejecta mass and kinetic energy of other 11 SNe studied by Taddia et al. (2018)⁴ and one ultra-stripped envelope SN iPTF14gqr (De et al. 2018). Fig. 3 presents a comparison of our results to those obtained using numerical modeling. Our estimation of ejecta mass (left panel) is consistent with the hydrodynamic calculation while the kinetic energy distribution (middle panel) shows a discrepancy. The right panel depicts a histogram of the ratios of quantities obtained by our estimates to those by numerical modeling. The mean and standard deviation of $\log(M_{\text{ej}}/M_{\text{ej,Hy}})$ are -0.24 and 0.24 , respectively. Thus our estimation nicely agrees with that by hydrodynamic modeling with an accuracy of a factor 2. The distribution of $\log(E_{\text{kin}}/E_{\text{kin,Hy}})$ has a mean and standard deviation of -0.11 and 0.56 , respectively. This poorer agreement is because the kinetic energy is more sensitive to the estimate of the velocity which in turn depends on the explosion time (see error bars in right panel of Fig. 3).

We briefly mention an interesting result of our method concerning the density profile of SN ejecta. Since we estimate the density ρ_{c} for each observation time t , we can reconstruct the density profile of the ejecta by correcting the expansion effect ρt^3 . Fig. 4 depicts a reconstructed density profile of SN 2004fe in the velocity coordinate. The profile could be described by a broken-power-law and it is consistent with the expected structure (Chevalier & Soker 1989; Matzner & McKee 1999). These works show that the power-law indexes of the inner (slow) and outer (fast) parts are ~ -1 and ~ -10 , respectively. As shown in Fig. 4, the inner-part’s index of ~ -1.5 agrees with their results, while the outer part has a shallower slope similar to that given by Sakurai (1960), ≈ -5.26 .

⁴ We exclude SN 2009ca because its luminosity is unusually large among this sample and it might be an outlier.

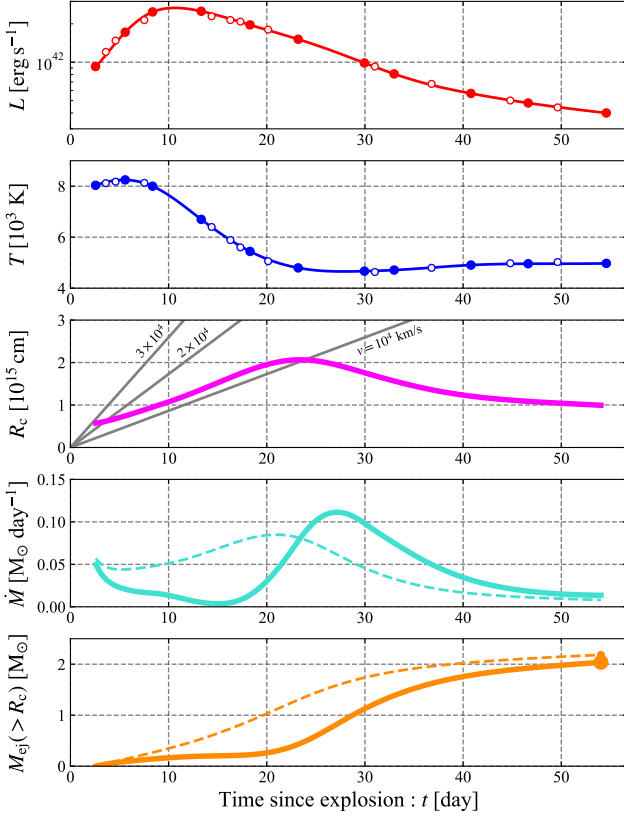


Figure 2. The observed luminosity, temperature, estimated color radius R_c ($> R_d$), mass outflow rate, and ejecta mass above the color radius of SN 2004fe. The observables are taken from figure 12 in Taddia et al. 2018. In the panel of R_c , the gray lines show the distance of the shells expanding with constant velocities of $v = 10^4$, 2×10^4 , and 3×10^4 km s $^{-1}$. For \dot{M} and M_{ej} , we also show the quantities neglecting the term dR/dt ($f_c = 1$) with dashed curves. Including the term dR/dt in Eq. (3), the mass outflow rate is enhanced (suppressed) before (after) the peak of R_c (≈ 25 day). Note that to obtain smooth fitting curves we used only the solid data points.

Table 1. Ejecta mass and kinetic energy of type Ic SNe estimated by our method (M_{ej} , E_{kin}). We also show their ratios to those obtained by hydrodynamical modeling ($M_{ej,Hy}$, $E_{kin,Hy}$) by Taddia et al. 2018. Only the uncertainty of the explosion time is included to calculate the errors.

Event	M_{ej} [M_{\odot}]	$M_{ej}/M_{ej,Hy}$	E_{kin} [10^{51} erg]	$E_{kin}/E_{kin,Hy}$
SN 2004fe	$2.0^{+0.3}_{-0.3}$	$0.8^{+0.1}_{-0.1}$	$1.5^{+3.4}_{-0.9}$	$0.8^{+1.7}_{-0.4}$
SN 2004gt	$1.3^{+0.2}_{-0.2}$	$0.4^{+0.1}_{-0.1}$	$0.3^{+0.2}_{-0.1}$	$0.09^{+0.1}_{-0.03}$
SN 2005aw	$1.6^{+0.2}_{-0.2}$	$0.4^{+0.1}_{-0.04}$	$0.6^{+0.5}_{-0.2}$	$0.3^{+0.2}_{-0.1}$
SN 2005em	$2.8^{+0.5}_{-0.5}$	$2.6^{+0.5}_{-0.4}$	$3.9^{+4.6}_{-1.9}$	$15.5^{+18.2}_{-7.6}$
SN 2006ir	$3.2^{+0.2}_{-0.2}$	$0.7^{+0.04}_{-0.03}$	$1.2^{+0.4}_{-0.3}$	$0.5^{+0.2}_{-0.1}$
SN 2007ag	$1.5^{+0.3}_{-0.3}$	$0.6^{+0.1}_{-0.1}$	$0.9^{+0.6}_{-0.2}$	$1.5^{+1.1}_{-0.1}$
SN 2007hn	$0.8^{+0.3}_{-0.3}$	$0.5^{+0.2}_{-0.2}$	$1.6^{+1.8}_{-0.9}$	$3.9^{+0.6}_{-2.3}$
SN 2007rz*	$1.3^{+0.1}_{-0.1}$	$0.7^{+0.1}_{-0.1}$	$0.6^{+0.3}_{-0.2}$	$0.6^{+0.3}_{-0.2}$
SN 2008hh	$1.9^{+0.4}_{-0.3}$	$0.5^{+0.1}_{-0.1}$	$1.7^{+1.5}_{-0.7}$	$0.6^{+0.5}_{-0.2}$
SN 2009bb	$2.7^{+0.1}_{-0.1}$	$0.6^{+0.02}_{-0.02}$	$1.6^{+0.2}_{-0.2}$	$0.2^{+0.03}_{-0.02}$
SN 2009dp	$1.0^{+0.4}_{-0.2}$	$0.5^{+0.2}_{-0.1}$	$1.3^{+2.3}_{-0.7}$	$1.3^{+2.3}_{-0.7}$
SN 2009dt	$0.4^{+0.2}_{-0.1}$	$0.2^{+0.1}_{-0.1}$	$0.4^{+0.5}_{-0.2}$	$1.0^{+1.2}_{-0.5}$
SN 14gqr*	0.08	0.36	0.06	0.45

* $M_{ej,Hy}$ and $E_{kin,Hy}$ are not available and we use the values given by Arnett’s rule (Arnett 1980, 1982).

4 EJECTA MASS OF OPTICAL TDES

We turn now to our original goal estimating the ejecta mass of optical TDEs. We focus on the “reprocessing-outflow” model, where we can assume that a quasi-spherical wind is launched and the thermal photons reprocessed by this wind diffuse out from the outflow (Metzger & Stone 2016; Roth et al. 2016; Roth & Kasen 2018; Dai et al. 2018; Lu & Bonnerot 2020; Piro & Lu 2020).

Consider an optical TDE whose luminosity and temperature are known as a function of time. We integrate Eqs. (9) and (14) up to the end of the observation time. We use the electron scattering opacity of $\kappa_{es} = 0.35$ cm 2 g $^{-1}$ and the Kramers’ absorption opacity with $\kappa_0 = 4 \times 10^{25}$ (see Appendix A) assuming that the ejecta’s chemical composition is solar. Different from the homologously-expanding SN ejecta, we do not have here a good estimate of the velocity. As the system is quasi-stationary the outflow may be launched with a constant velocity, we fix the velocity and vary it as a parameter (we will return to this point later). Similarly, we neglect the term of dR/dt in the mass outflow rate, which becomes $\sim 10^{15-16}$ cm/100 days $\approx 10^{3-4}$ km s $^{-1}$ for a typical event. This simplification gives us a conservative estimate of ejecta mass (smaller mass) because the radii R_d and R_c shrink during observations, increasing \dot{M} .

Fig. 5 depicts the time evolution of the observables (L and T), radius, mass outflow rate, and ejecta mass beyond the radius for ASASSN-14ae, 14li, and 15oi (as Fig. 2) for an assumed fixed velocity of $v = 10^4$ km s $^{-1}$. In this case, the diffusion radius is always larger than the color radius $R_d > R_c$. The ejecta mass exceeds a solar mass as early as 5 – 30 days after the discovery.

Fig 6 depicts the ejecta mass of 27 optical TDEs (data are taken from Hung et al. 2017; van Velzen et al. 2020a) 5 calculated for different velocities ranging from $v = 3 \times 10^2$ to 3×10^4 km s $^{-1}$. The estimated ejecta mass peaks at the critical velocity of $v_{crit} \approx 10^4$ km s $^{-1}$ for which $R_d = R_c$ (Note the dependences of the outflow rate, $\dot{M} \propto v$ ($\propto v^{-1/2}$) for $v < v_{crit}$ ($v > v_{crit}$), see also Eq. (20) and Shen et al. 2015). Interestingly this critical velocity is comparable to those suggested by line broadening (Arcavi et al. 2014 but see also Roth et al. 2016; Roth & Kasen 2018 for other mechanism giving the observed line broadening) and expected in the “reprocessing-outflow” model (Metzger & Stone 2016). For most TDEs, the ejecta mass is larger than a solar mass for velocities of $v \approx 3 \times 10^3 - 10^4$ km s $^{-1}$ even in our conservative calculation. The mass is smaller than a solar mass if the ejecta velocity is lower than $v \lesssim 10^{2-3}$ km s $^{-1}$. Such low velocities lower than the escape velocity are unlikely in the system powered by a super-Eddington disk. Moreover, in this case the ejecta’s kinetic energy is as small as $E_{kin} \lesssim 10^{49}$ erg, and this outflow does not solve the “inverse energy crisis”.

A way to estimate the velocity is adopting the escape velocity at the radius $v_{esc}(R) = \sqrt{GM_{BH}/R}$, which is a lower limit if the sonic radius is inside the radius $< R$ (Shen et al. 2016). Here G is the gravitational constant and M_{BH} is the BH mass. Using Eqs. (7) and

5 We exclude AT2018iuh which is most likely not a TDE (see Ryu et al. 2020). For example, its luminosity declines much slower than all other TDEs. The corresponding estimated ejecta mass $\sim 10^2 M_{\odot}$, is indeed unreasonably large.

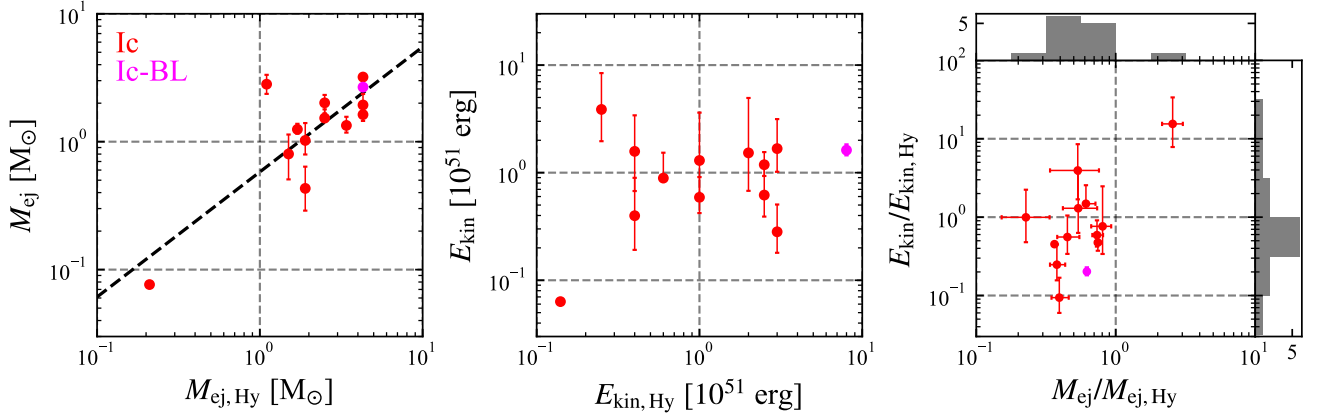


Figure 3. (Left) A comparison of ejecta mass estimated by our method M_{ej} with those obtained by hydrodynamical modeling, $M_{\text{ej,Hy}}$ (Taddia et al. 2018). The red and magenta points show the type Ic and broad-line Ic (Ic-BL) SNe, respectively. The black dashed line shows the best fit to the points: $\log M_{\text{ej}} = 0.98 \log M_{\text{ej,Hy}} - 0.24$. (Middle) Same as for the left panel but for the kinetic energy. (Right) The distribution of the ratios, $M_{\text{ej}}/M_{\text{ej,Hy}}$ and $E_{\text{kin}}/E_{\text{kin,Hy}}$. The mean and standard deviation of the distributions in log space are -0.24 and 0.24 for the mass ratio, and -0.11 and 0.56 for the energy ratio, respectively.

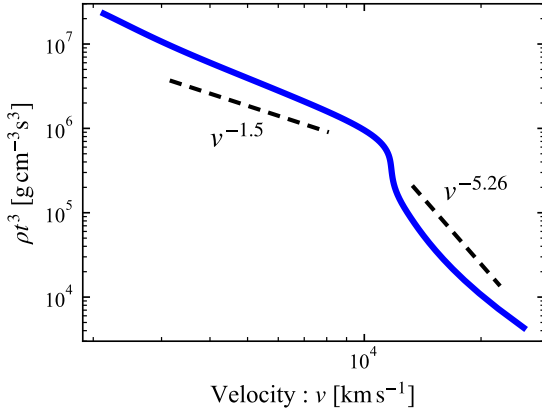


Figure 4. Density profile of SN 2004fe in the velocity coordinate reconstructed by correcting the expansion effect (ρr^3). The profile is described by a broken-power-law function consistent with Chevalier & Soker 1989; Matzner & McKee 1999. The inner part has a slope $\rho \propto v^{-1.5}$ and the outer part has a similar power-law index to that expected for Sakurai’s solution: $\rho \propto v^{-5.26}$ (Sakurai 1960).

(13), the escape velocities at radii R_d and R_c are;

$$v_{\text{esc}}(R_d) \approx \left(\frac{2^4 \pi \sigma_{\text{SB}} G^2 M_{\text{BH}}^2}{3c} \right)^{1/3} L^{-1/3} T^{4/3} \quad (28)$$

$$\approx 840 \text{ km s}^{-1} M_{\text{BH},6.5}^{2/3} L_{44}^{-1/3} T_4^{4/3},$$

$$v_{\text{esc}}(R_c) \approx \left(\frac{2^{12} \pi^3 \sigma_{\text{SB}}^3 \kappa_0 G^5 M_{\text{BH}}^5}{3^3 \kappa_{\text{es}}^2} \right)^{1/10} L^{-3/10} T^{17/20} \quad (29)$$

$$\approx 1900 \text{ km s}^{-1} M_{\text{BH},6.5}^{1/2} L_{44}^{-3/10} T_4^{17/20},$$

where we use $M_{\text{BH},6.5} = M_{\text{BH}}/(10^{6.5} M_{\odot})$. The resulting typical escape velocities are $v_{\text{esc}} \sim 10^3 \text{ km s}^{-1}$. Plugging Eqs. (28) and (29)

into Eqs. (9) and (14) we find the corresponding mass outflow rates:

$$\dot{M}_d \approx \left(\frac{3^2 \pi c^5}{2^2 \kappa_{\text{es}}^3 \sigma_{\text{SB}}^2 G M_{\text{BH}}} \right)^{1/3} L^{2/3} T^{-8/3} \quad (30)$$

$$\approx 2.9 M_{\odot} \text{ day}^{-1} M_{\text{BH},6.5}^{-1/3} L_{44}^{2/3} T_4^{-8/3},$$

$$\dot{M}_c \approx \left(\frac{3\pi G M_{\text{BH}}}{\kappa_0 \sigma_{\text{SB}}} \right)^{1/2} L^{1/2} T^{-1/4} \quad (31)$$

$$\approx 1.9 \times 10^{-1} M_{\odot} \text{ day}^{-1} M_{\text{BH},6.5}^{1/2} L_{44}^{1/2} T_4^{-1/4}.$$

Fig. 7 depicts the estimated ejecta mass and kinetic energy for $v = v_{\text{esc}}(R)$ adopting the BH mass listed in Hung et al. (2017) or $10^{6.5} M_{\odot}$ when it is not available. The resulting ejecta mass are larger than a solar mass.

Finally, we comment on the results by Piro & Lu (2020). These authors updated the formalism of Metzger & Stone (2016). Assuming density and temperature profiles, they reproduced a TDE light curve with ejecta mass of $M_{\text{ej}} = 0.5 M_{\odot}$. However, they obtained a luminosity of $\sim 10^{43} \text{ erg s}^{-1}$ and temperature $\sim 10^5 \text{ K}$ (see their figure 5), which are inconsistent with those observed for typical TDEs: $\sim 10^{44} \text{ erg s}^{-1}$ and $\approx 3 \times 10^4 \text{ K}$. Using such a low luminosity and high temperature we also obtain an ejecta mass that is less than a solar mass.

5 SUMMARY

We present here a new method, based on earlier ideas of Shen et al. (2015) and Piro & Lu (2020), to estimate the ejecta mass of optical transients that involve a quasi-spherically expanding outflow and have a thermal spectrum. To test the method, we calculated the ejecta mass of type Ic SNe and confirmed that it gives a reasonable estimate with an accuracy of a factor 2. Interestingly, for a well-observed SN we can also explore the velocity and density structure of the ejecta and we find a density profile consistent with the expected structure (Sakurai 1960; Chevalier & Soker 1989; Matzner & McKee 1999).

Assuming the “reprocessing-outflow” model in which TDEs are powered by a compact source (accretion disk) whose soft X-ray emission is reprocessed at a larger radius to optical/UV emission (Metzger

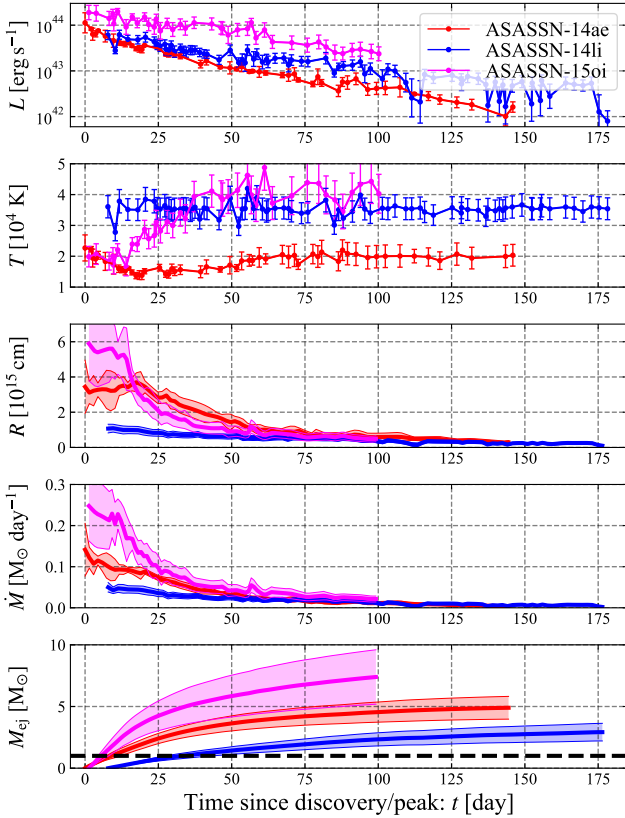


Figure 5. Same as Fig. 2 but for optical TDEs ASASSN-14as (red), 14li (blue), and 15oi (magenta) for a fixed velocity of $v = 10^4 \text{ km s}^{-1}$. The observables are taken from Holoien et al. 2014, 2016a,b. The shaded regions in the bottom three panels denote the error range calculated when the observational statistical errors in upper two panels is taken into account. The ejecta mass exceeds M_{\odot} (black dashed line), as early as 5-30 days after the discovery. As noticed by Piro & Lu 2020, R_d is larger than the black-body radius $R_{\text{bb}} \equiv (L/4\pi\sigma_{\text{SB}}T^4)^{1/2}$, that is commonly used to estimate the size of ejecta (see e.g., Hung et al. 2017). This is not inconsistent because in the situation we consider R_{bb} has nothing to do with the emission process (see also Nakar & Sari 2010).

& Stone 2016; Roth et al. 2016; Roth & Kasen 2018; Dai et al. 2018; Lu & Bonnerot 2020; Piro & Lu 2020) we apply this method to optical TDEs. Unlike SNe the outflow is not expanding homogeneously and it is in a quasi-steady state. As a result the velocities are unknown. While observations show line broadening corresponding to $v \sim 10^4 \text{ km s}^{-1}$ (e.g., Arcavi et al. 2014), it is not clear that this reflects the outflow velocity (Roth et al. 2016; Roth & Kasen 2018). Hence, we assume different ejecta velocities and explore the dependence of the results on the adopted velocity. As we expect a quasi-steady state outflow, the assumption of a constant velocity is reasonable. Alternatively following hydrodynamic modeling by Shen et al. (2016) we use the escape velocity.

We find reasonable ejecta masses (less than \sim solar) only for ejecta velocities less than about thousand km s^{-1} . The corresponding ejecta kinetic energy is smaller than 10^{49} erg, which is well below the expected value ($\sim 10^{52-53}$ erg) if the ejecta are launched from the compact source and does not resolve the inverse energy crisis. For larger velocities comparable to those inferred from the line width or implied by the escape velocity, $v \simeq 3 \times 10^3 - 10^4 \text{ km s}^{-1}$, the ejected mass is significantly larger than solar. These results cast some doubt

on the overall picture of a wide range of “reprocessing-outflow” model. We find that the resulting wind would be either too massive or if it is not massive it will not carry sufficient energy to provide the missing “energy sink”.

Some reprocessing models (Loeb & Ulmer 1997; Guillochon et al. 2014; Coughlin & Begelman 2014; Roth et al. 2016) assume a quasi-static layer of poorly circularized debris reprocesses the ionizing continuum from the (efficiently circularized) inner accretion disk. As the assumed velocities are small in this case the ejecta mass estimates do not pose a problem. However, the “inverse energy crisis” remains here as it is not clear how does the excess energy disappear.

There are several caveats in our results. The first is the assumption of spherical geometry. Clearly the configuration is not spherical. However, while such deviations are natural in a TDE, we expect that if a deviation is on a large angular scale it could be taken into account by considering the fraction of the solid angle subtended by the outflow. This will not change quantitatively our results. We expect that only large deviations such as a formation of a jet would change our conclusions significantly. van Velzen et al. (2013) use late-time radio observations to put an upper limits on Sw J1644 like events (jetted TDEs). They find that at high probability all seven events that they analyzed did not have $> 10^{52}$ erg jets. A more detailed analysis would likely yield much stronger limits.

A second caveat is the assumption that the emission is thermalized and is well described by a single temperature black-body. While this is natural if the emission is indeed reprocessed by optically thick matter, lacking a detailed measurement of the spectrum it is still unclear. Moreover, the temperature is usually determined only by using multi-band photometry. If for the given luminosity the true temperature is larger by a factor of 3 the ejecta mass would decrease by a factor of $\sim 3 - 10$ (see Eqs. 9 and 14), leading possibly to acceptable solution. However, if the luminosity is also varied to reflect the higher temperature the mass estimate remains valid.

To conclude, we presented here a simple generic method to estimate the outflow from quasi-spherical optical transients. The method is valid for events that are optically thick and when the luminosity and temperature have been measured as a function of time. To test the method we have applied it to SNe finding an encouraging agreement with more detailed calculations. When applying it to optical TDEs, we find that if indeed the observed emission is thermal and it arises from a compact accretion disk then the resulting mass of the outflow is too large. This poses a problem for the “reprocessing-outflow” model. This problem does not arise in models in which an outflow is not expected such as the alternative “outer shocks” and in variants of the reprocessing model considering a static envelop. With numerous on-going and forthcoming observational campaigns aiming at exploring the transient universe it will be interesting to analyze in future work other optical transients using this method.

ACKNOWLEDGMENTS

We thanks Iair Arcavi, Chi-Ho Chan, Tamar Faran, Julian Krolik, Keiichi Maeda, Kartick Sarkar, Nicholas Stone, and Masaomi Tanaka for fruitful discussions and helpful comments. We also appreciate an anonymous referee for helpful suggestions. This work is supported in part by JSPS Postdoctoral Fellowship, Kakenhi No. 19J00214 (T.M.) and by ERC advanced grant “TRex” (T.P.).

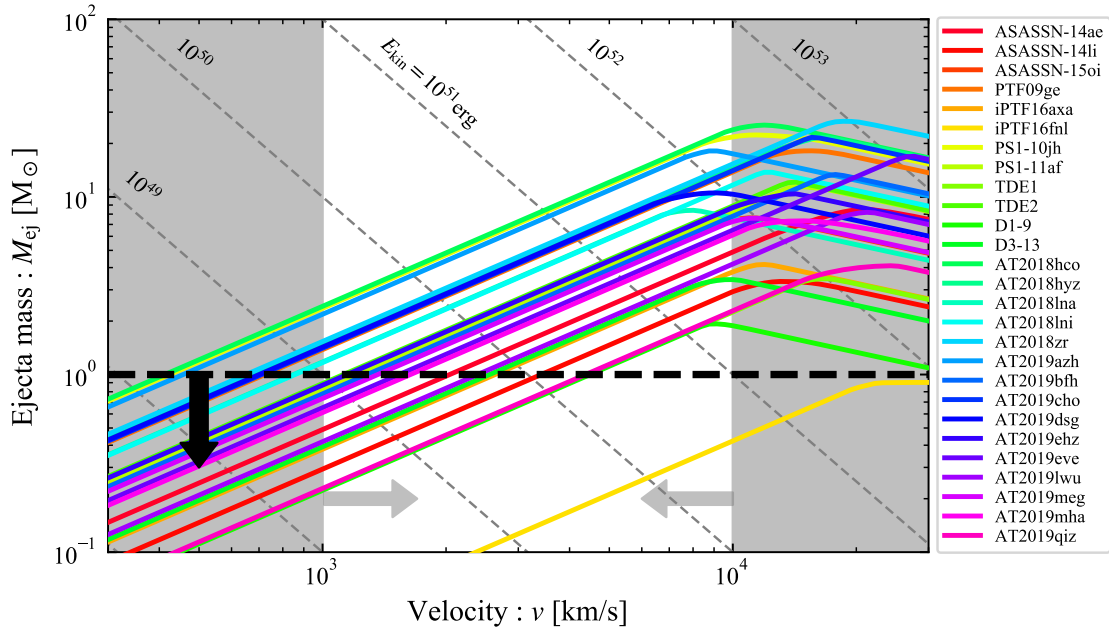


Figure 6. Estimated ejecta mass of observed optical TDEs for different ejecta velocities. The gray dashed lines show the kinetic energy at each velocity. As a reference the black dashed line denotes M_{\odot} . Typical TDE debris should be below this line. For each event, the ejecta mass has a peak at the critical velocity $v_{\text{crit}} \approx 3 \times 10^3 - 10^4 \text{ km s}^{-1}$ (Eq. 17). When $v < v_{\text{crit}}$ ($v > v_{\text{crit}}$), the color radius is larger (smaller) than the diffusion radius, $R_d < R_c$ ($R_c < R_d$). For the ejecta mass to be sufficiently small, the velocity should be smaller than $v \sim 10^{2-3} \text{ km s}^{-1}$. The gray shaded regions show velocities excluded by the observations of line widths $v \lesssim 10^4 \text{ km s}^{-1}$ or lower than the escape velocity $v_{\text{esc}} \approx 10^3 \text{ km s}^{-1}$.

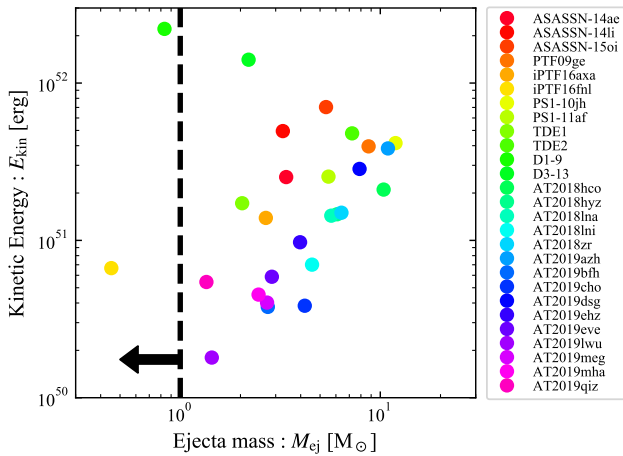


Figure 7. The ejecta mass and the kinetic energy calculated by setting the velocity to the escape velocity at R_d or R_c , $v = v_{\text{esc}}(R)$.

DATA AVAILABILITY

The data underlying this article will be shared on reasonable request to the corresponding author.

APPENDIX A: ABSORPTION OPACITY

The Planck-mean opacity is defined by

$$\kappa_a = \frac{\int_0^{\infty} \kappa_{a,\nu} B_{\nu}(T) d\nu}{\int_0^{\infty} B_{\nu}(T) d\nu}, \quad (\text{A1})$$

where $\kappa_{a,\nu}$ and $B_{\nu}(T)$ are the frequency-dependent absorption opacity and the Planck function, respectively. We calculate $\kappa_{a,\nu}$ using the open-source code CLOUDY.⁶ For TDE ejecta, we include only continuum opacity (free-free and bound-free absorption) because for TDE temperature $\gtrsim 10^4 \text{ K}$ the bound-bound transitions are typically unimportant. Figs. A1 depicts the resulting Planck-mean opacity for TDEs (solar abundance). The absorption opacity is well approximated by the Kramers' opacity formula $\kappa_a = \kappa_0 \rho T^{-7/2}$ with the normalization of $\kappa_0 = 4 \times 10^{25}$. Note that this value is about 10 times larger than the one adopted to approximate the Rosseland-mean opacity.

For type Ic SN ejecta, bound-bound transitions may dominate the absorption opacity whose dependence on density and temperature is less clear. In analytical light-curve modeling of type Ia SNe, a constant opacity is usually adopted (e.g., Piro & Nakar 2014). Kasen et al. (2013) present a sample of opacity calculation for silicon, which shows that the opacity does not depend on temperature sensitively (see their figure 6). Following the calculation by Dessart et al. (2015) (see their figure 24) we adopt here a constant Planck-mean opacity with $\kappa_a = 0.01 \text{ cm}^2 \text{ g}^{-1}$.

REFERENCES

Arcavi I., et al., 2014, *ApJ*, 793, 38

⁶ Version 17.01 of the code last described (Ferland et al. 2017).

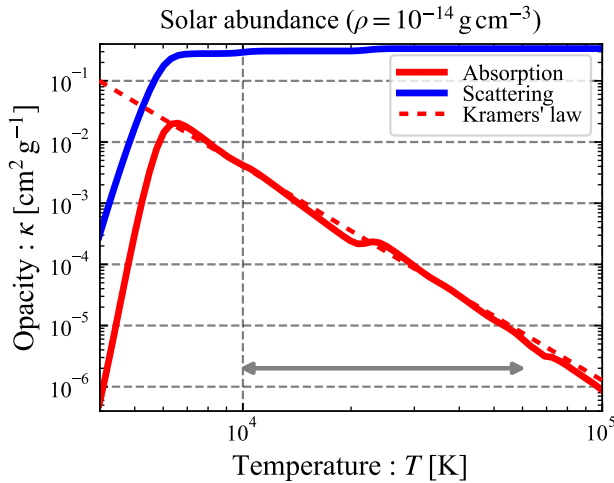


Figure A1. Absorption and scattering opacities for solar abundance ejecta (relevant to TDEs) calculated using CLOUDY. The absorption opacity is calculated by averaging frequency-dependent continuum (free-free and bound-free) opacity with Planck function (Planck-mean). The dashed line shows the Kramers' opacity adopted in our calculation, which well approximates the absorption opacity in the TDE temperature range (gray arrow).

Arnett W. D., 1980, *ApJ*, **237**, 541
 Arnett W. D., 1982, *ApJ*, **253**, 775
 Bade N., Komossa S., Dahlem M., 1996, *A&A*, **309**, L35
 Bersten M. C., Benvenuto O., Hamuy M., 2011, *ApJ*, **729**, 61
 Bersten M. C., et al., 2012, *ApJ*, **757**, 31
 Blagorodnova N., et al., 2017, *ApJ*, **844**, 46
 Blagorodnova N., et al., 2019, *ApJ*, **873**, 92
 Blandford R. D., Begelman M. C., 1999, *MNRAS*, **303**, L1
 Brandt W. N., Pounds K. A., Fink H., 1995, *MNRAS*, **273**, L47
 Chevalier R. A., Soker N., 1989, *ApJ*, **341**, 867
 Chornock R., et al., 2014, *ApJ*, **780**, 44
 Coughlin E. R., Begelman M. C., 2014, *ApJ*, **781**, 82
 Dai L., McKinney J. C., Roth N., Ramirez-Ruiz E., Miller M. C., 2018, *ApJ*, **859**, L20
 De K., et al., 2018, *Science*, **362**, 201
 Dessart L., Hillier D. J., Livne E., Yoon S.-C., Woosley S., Waldman R., Langer N., 2011, *MNRAS*, **414**, 2985
 Dessart L., Hillier D. J., Woosley S., Livne E., Waldman R., Yoon S.-C., Langer N., 2015, *MNRAS*, **453**, 2189
 Donato D., et al., 2014, *ApJ*, **781**, 59
 Esquej P., Saxton R. D., Freyberg M. J., Read A. M., Altieri B., Sanchez-Portal M., Hasinger G., 2007, *A&A*, **462**, L49
 Esquej P., et al., 2008, *A&A*, **489**, 543
 Faran T., Goldfriend T., Nakar E., Sari R., 2019, *ApJ*, **879**, 20
 Ferland G. J., et al., 2017, *Rev. Mex. Astron. Astrofis.*, **53**, 385
 Gezari S., et al., 2006, *ApJ*, **653**, L25
 Gezari S., et al., 2008, *ApJ*, **676**, 944
 Gezari S., et al., 2012, *Nature*, **485**, 217
 Grassberg E. K., Imshennik V. S., Nadyozhin D. K., 1971, *Ap&SS*, **10**, 28
 Greiner J., Schwarz R., Zharikov S., Orlo M., 2000, *A&A*, **362**, L25
 Grupe D., Beuermann K., Mannheim K., Bade N., Thomas H. C., de Martino D., Schwope A., 1995, *A&A*, **299**, L5
 Grupe D., Thomas H. C., Leighly K. M., 1999, *A&A*, **350**, L31
 Guillochon J., Manukian H., Ramirez-Ruiz E., 2014, *ApJ*, **783**, 23
 Holoien T. W. S., et al., 2014, *MNRAS*, **445**, 3263
 Holoien T. W. S., et al., 2016a, *MNRAS*, **455**, 2918
 Holoien T. W. S., et al., 2016b, *MNRAS*, **463**, 3813
 Hung T., et al., 2017, *ApJ*, **842**, 29
 Kasen D., Badnell N. R., Barnes J., 2013, *ApJ*, **774**, 25

Komossa S., 2015, *Journal of High Energy Astrophysics*, **7**, 148
 Komossa S., Bade N., 1999, *A&A*, **343**, 775
 Komossa S., Greiner J., 1999, *A&A*, **349**, L45
 Krolik J. H., Piran T., 2012, *ApJ*, **749**, 92
 Krolik J., Piran T., Svirski G., Cheng R. M., 2016, *ApJ*, **827**, 127
 Lodato G., Rossi E. M., 2011, *MNRAS*, **410**, 359
 Loeb A., Ulmer A., 1997, *ApJ*, **489**, 573
 Lu W., Bonnerot C., 2020, *MNRAS*, **492**, 686
 Lu W., Kumar P., 2018, *ApJ*, **865**, 128
 Lyman J. D., Bersier D., James P. A., Mazzali P. A., Eldridge J. J., Fraser M., Pian E., 2016, *MNRAS*, **457**, 328
 Maksym W. P., Ulmer M. P., Eracleous M. C., Guennou L., Ho L. C., 2013, *MNRAS*, **435**, 1904
 Matzner C. D., McKee C. F., 1999, *ApJ*, **510**, 379
 Metzger B. D., Stone N. C., 2016, *MNRAS*, **461**, 948
 Nakar E., Sari R., 2010, *ApJ*, **725**, 904
 Nicholl M., et al., 2020, arXiv e-prints, p. arXiv:2006.02454
 Phinney E. S., 1989, in Morris M., ed., *IAU Symposium Vol. 136, The Center of the Galaxy*, p. 543
 Piran T., Svirski G., Krolik J., Cheng R. M., Shiokawa H., 2015, *ApJ*, **806**, 164
 Piro A. L., Lu W., 2020, *ApJ*, **894**, 2
 Piro A. L., Morozova V. S., 2014, *ApJ*, **792**, L11
 Piro A. L., Nakar E., 2014, *ApJ*, **784**, 85
 Popov D. V., 1993, *ApJ*, **414**, 712
 Rees M. J., 1988, *Nature*, **333**, 523
 Roth N., Kasen D., 2018, *ApJ*, **855**, 54
 Roth N., Kasen D., Guillochon J., Ramirez-Ruiz E., 2016, *ApJ*, **827**, 3
 Rybicki G. B., Lightman A. P., 1979, *Radiative processes in astrophysics*
 Ryu T., Krolik J., Piran T., 2020, arXiv e-prints, p. arXiv:2007.13765
 Sakurai A., 1960, *Commun. Pure Appl. Math*, **13**, 353
 Shen R. F., Barniol Duran R., Nakar E., Piran T., 2015, *MNRAS*, **447**, L60
 Shen R.-F., Nakar E., Piran T., 2016, *MNRAS*, **459**, 171
 Shiokawa H., Krolik J. H., Cheng R. M., Piran T., Noble S. C., 2015, *ApJ*, **804**, 85
 Stone N. C., Metzger B. D., 2016, *MNRAS*, **455**, 859
 Strubbe L. E., Quataert E., 2009, *MNRAS*, **400**, 2070
 Svirski G., Piran T., Krolik J., 2017, *MNRAS*, **467**, 1426
 Taddia F., et al., 2018, *A&A*, **609**, A136
 Uno K., Maeda K., 2020, *ApJ*, **897**, 156
 van Velzen S., et al., 2011, *ApJ*, **741**, 73
 van Velzen S., Frail D. A., Körding E., Falcke H., 2013, *A&A*, **552**, A5
 van Velzen S., et al., 2020a, arXiv e-prints, p. arXiv:2001.01409
 van Velzen S., Holoien T. W. S., Onori F., Hung T., Arcavi I., 2020b, arXiv e-prints, p. arXiv:2008.05461

This paper has been typeset from a $\text{\TeX}/\text{\LaTeX}$ file prepared by the author.